Elasticity of hydrogen to 24 GPa from single-crystal Brillouin scattering and synchrotron x-ray diffraction

Chang-sheng Zha, Thomas S. Duffy, Ho-kwang Mao, and Russell J. Hemley

Geophysical Laboratory and Center for High-Pressure Research, Carnegie Institution of Washington,
5251 Broad Branch Road, NW, Washington, D.C. 20015

We have developed a technique for studying the elasticity of single crystals of solid hydrogen and related materials at very high pressures and used the method to determine the second-order elastic moduli of single-crystal n-type hydrogen to 24 GPa at 295 K. The method involves the measurement of acoustic velocities as a function of crystallographic direction by Brillouin scattering in a diamond anvil cell with the orientation of the single crystals determined by synchrotron x-ray diffraction. Between 6 and 24 GPa, the adiabatic bulk modulus of H_2 increases by more than a factor of 3 and the shear modulus increases by more than a factor of 4. The acoustic anisotropy of hydrogen decreases from 11% to 6% for compressional waves and from 23% to 14% for shear waves. The data are also used to calculate thermodynamic properties of hydrogen at high pressures. By including the observed velocity anisotropy, the equation of state of H_2 derived from Brillouin data is in agreement with previous results derived solely from x-ray diffraction.

I. INTRODUCTION

The behavior of dense solid hydrogen is currently of great interest in view of the variety of changes induced in the solid as a function of pressure. With increasing pressure, solid hydrogen maintains its molecular character as it evolves from a low-density quantum solid to a high-density state with increasing intermolecular interactions.[1,2] At sufficiently high pressure, the molecular solid is expected to transform to a higher-density monoatomic metallic form. In addition, at intermediate densities, it is possible that metallic, semimetallic, or partially delocalized states are stable within the molecular solid (i.e., with no depairing of the protons).[3] Understanding this sequence of pressure-induced transitions requires detailed measurements using a wide variety of experimental probes at very high pressure.

Diamond cell experiments carried out during the past 5 years have provided a growing database of physical and chemical properties of the solid needed to address this question.[3,4] The lattice structure of the solid has been established by diffraction experiments.[5,6] In particular, synchrotron x-ray-diffraction measurements[5–7] reveal that n- type hydrogen (0.75 mol fraction ortho-H_2) crystallizes in the hcp structure to at least 42 GPa (at room temperature). The dynamical properties and state of molecular bonding have been probed by vibrational Raman scattering and infrared spectroscopy. Measurements on the vibrons demonstrate that the solid remains molecular well into the megabar range (>200 GPa).[8–15] Further, low-frequency Raman measurements of rotons and lattice modes demonstrate that H_2 persists in states of rotational disorder within the hcp structure to >100 GPa, with D_2 undergoing transitions at lower pressures.[16–18] Constraints on the electronic properties at high pressure have been obtained from index of refraction measurements,[19–21] conventional optical absorption and reflectivity,[22–25] and more recently, synchrotron infrared spectroscopy.[14,15]

Measurements of the high-pressure elastic properties of hydrogen provide information on the anisotropy, equation of state, and thermodynamic properties of this material. Indeed, the determination of the anisotropy in the solid at very high pressure is important for characterizing optical spectra (e.g., Ref. 25). Brillouin scattering provides a means for probing the elastic properties of microscopic samples held at high pressure in a diamond-anvil cell. In this technique, the frequency shift of laser light scattered by thermally generated sound waves is used to determine acoustic velocities. The technique was first applied to hydrogen in 1980 by Brody *et al.*[26] and Shimizu *et al.*,[27] who studied the material to 20 GPa. Despite the importance of the technique, there have been comparatively few high-pressure Brillouin measurements relative to other spectroscopic techniques carried out with the diamond cell. Moreover, to our knowledge, there have been no studies of hydrogen to date since the studies described in Refs. 26 and 27, which were performed prior to the determination of the crystal structure.

Progress in the study of the high-pressure elastic properties of crystalline materials with Brillouin scattering has been reviewed by Polian.[28] The nature of the diamond cell imposes a number of restrictions on the use of the Brillouin technique with this device. Specialized diamond cells with large openings allow acoustic velocities to be measured in a large number of directions, but the maximum pressure attainable is limited.[29] Traditional cells restrict the accessible scattering geometries such that only a few known crystal directions can be probed[30,31] or, in the case of the backscattering geometry, the refractive index must be known independently to obtain the acoustic velocity from the measured frequency

shift.[28] A further limitation of backscattering is that nor-
mally only the longitudinal phonons are detectable.
Clearly, a complete determination of elasticity requires
the use of several different scattering geometries together
with high-pressure cells that permit sufficient optical ac-
cess. Furthermore, for anisotropic crystals it is essential
that the orientation of the crystals be determined. This is
a particular problem for materials that are gases or
liquids at ambient pressure and therefore cannot be easily
oriented when they solidify under high pressure.

In this study, we have developed a technique for study-
ing the elasticity of single crystals of solid hydrogen and
related materials at very high pressures in the diamond
cell. We combine Brillouin scattering measurements as a
function of crystallographic direction with the orienta-
tion and characterization of the number of single crystals
determined by synchrotron x-ray-diffraction techniques.
This method enables us to determine the elastic constants
of a noncubic crystal grown in the diamond cell. By
fitting the velocity and orientation data we determine the
five second-order elastic moduli of hcp hydrogen to 24
GPa, and we obtain constraints on the thermodynamic
properties of the dense solid. In addition, analysis of the
data shows that the equation of state determined by Bril-
louin scattering is in good agreement with that deter-
mined directly by x-ray diffraction.

The remainder of the paper is organized as follows. In
Sec. II, we present an overview of the technique. The re-
sults of the measurements are given in Sec. III. In Sec.
IV, we discuss the analysis of the velocity distribution
and the fitting procedure used to obtain the elastic modu-
li. In Sec. V, we discuss the thermodynamic properties,
and in Sec. VI the equation of state. Finally, our con-
clusions are presented in Sec. VII.

II. EXPERIMENTAL METHODS

Pure hydrogen gas and a single grain of ruby were
loaded into a 150-μm rhenium gasket hole of a large-
aperture Merrill-Bassett diamond cell.[32] The sample was
carefully pressurized above the room-temperature freez-
ing point (5.4 GPa) to form a single crystal.[33,34] Pres-
sures were obtained by measuring the frequency shift of
the R_1 fluorescence line of ruby.[35]

Brillouin scattering measurements were carried out
with a newly constructed spectrometer utilizing a six-pass
tandem Fabry-Perot interferometer.[36] A single-frequency
Ar^{+} laser was used as the excitation source. The system
was also designed to allow for a number of different
scattering geometries. The diamond cell was mounted on
a stage which allowed for x, y, and z translations, ω and χ
rotations, and x-axis tilts, and was designed such that the
loading axis was always in the scattering plane. A large
conical opening (aperture angle of 96°) in the diamond
cell allowed Brillouin frequency shift measurements to be
performed for a large number of directions by rotating χ
around the diamond cell axis. Most of the data were col-
lected using a 90° geometry (phonon direction parallel to
diamond culet) as shown in Fig. 1. The forward and
reflected backscattering wave vectors and phonon propa-
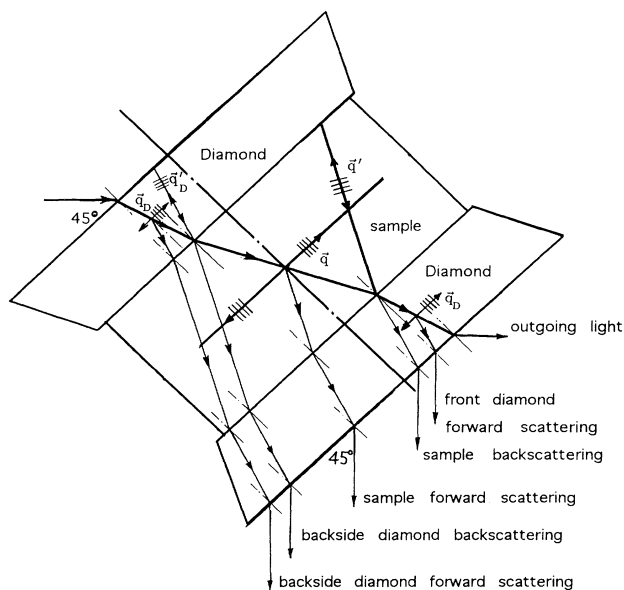gation directions are indicated. Additional measure-

FIG. 1. The 90° symmetric scattering geometry for the sam-
ple in the diamond cell. Several possible scattering geometries
are shown. q,q' represent the phonon wave vectors in the sam-
ple. q_D,q_D' represent the phonon wave vectors in the diamonds.

ments were performed using backscattering and asym-
metric (phonon directions not parallel to diamond culet)
geometries for determining the product of the refractive
index and velocity as well as for redundancy checks.

The crystallographic orientation was determined at
each pressure using synchrotron x-ray diffraction[5] at
beamline X17C of the National Synchrotron Light
Source, Brookhaven National Laboratory. We also
determined the optical thickness from measurements of
interference fringes.[19,20] These measurements were car-
ried out using polarized light on the single crystals of
known orientation to estimate the birefringence.

For 90° scattering, the Brillouin frequency shift, Δv, of
an optically isotropic material is related to the acoustic
velocity, V, and incident laser wavelength, λ_0, by the ex-
pression[37]

$$V = \frac{\Delta v \lambda_0}{\sqrt{2}} . \tag{1}$$

In order to estimate the uncertainty associated with using
this expression for an optically anisotropic solid, we used
polarized interference patterns, utilizing a linearly polar-
ized incident beam and an identically polarized analyzer,
to estimate the birefringence of solid hydrogen. From the
polarized interference pattern measured for known crys-
tal orientations, the difference in optical thickness, and
hence refractive index between the a and c crystal axes
was found to be approximately 1.5–2 % (at 9 GPa).
Neglect of this anisotropy introduces uncertainties in the
phonon directions and sound velocities that are well
within experimental errors. Combining the optical thick-
ness with the refractive index determined from Brillouin
scattering, the sample thickness was obtained.

III. RESULTS

Brillouin spectra of solid n-H_2 were collected for 15–20 separate crystallographic directions at each of six pressures between 6.4 and 23.6 GPa. A representative spectrum (phonon directed 21.3° from c axis) at 12.6 GPa is shown in Fig. 2. The quasi-compressional (V_P) and quasi-shear (V_S) waves from solid H_2 are indicated. Also shown are the reflected backscattering peaks and the signals from the diamond anvils. Single-crystal x-ray-diffraction measurements at 12.6 GPa revealed that the crystallographic c axis of the solid was located 18.3° from the diamond culet face with the a axis parallel to the culet. The sound velocity distribution in the a-c plane at 12.6 GPa is shown in Fig. 3. The lines are fits to the second-order elastic moduli, as discussed below.

As the pressure was increased, the sample recrystallized at each pressure until 15.9 GPa, at which point the crystal broke into two pieces with slightly different orientations. The orientation and number of crystals remained fixed during subsequent pressurization. The measured acoustic velocities as a function of crystallographic direction to 23.6 GPa are shown in Fig. 4. At 15.9 GPa and above, the velocities measured from the two crystals are entirely consistent and are shown together.

The intensity of the compressional wave Brillouin peaks was much greater than the intensity of the shear wave peaks, which accounts for the larger number and reduced scatter of the compressional measurements. For the shear waves, only the quasi-shear velocity was resolved, and we obtained no information on the pure shear velocity. A previous Brillouin scattering study[38] of H_2 at ambient pressure and 13.2 K was also unable to

FIG. 3. Acoustic velocity distribution in the a-c plane at 12.6 GPa (295 K). Symbols show experimental data points, solid lines are calculated velocities based on elastic constants. V_P, V_{S1}, V_{S2} represent quasi-compressional, pure shear, and quasi-shear velocities, respectively.

detect the pure shear mode. At 12.6 and 23.6 GPa, the compressional hydrogen Brillouin peaks were partially obscured by diamond shear and compressional wave peaks, respectively.

In the backscattering geometry, the measured frequency shift is proportional to the product of compressional velocity and refractive index.[28] By combining separate backscattering and 90° scattering experiments in which we made both the phonon propagation directions in the a plane (in which the refractive index and acoustic velocity
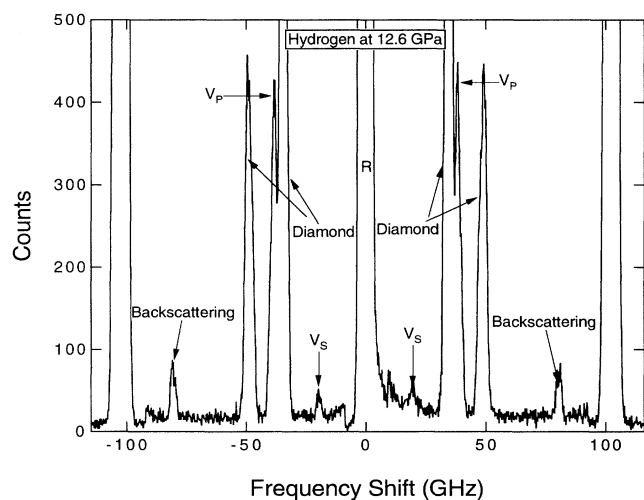

FIG. 2. Representative Brillouin scattering spectrum at 12.6 GPa. The central unshifted Rayleigh peak is labeled R. Additional Rayleigh peaks are at the right and left ends of the spectrum. The H_2 compressional and shear peaks are labeled V_P and V_S, respectively. Features near the base of the Rayleigh peaks are artifacts due to the acousto-optic modulator which attenuates the laser intensity when scanning through the Rayleigh peak.
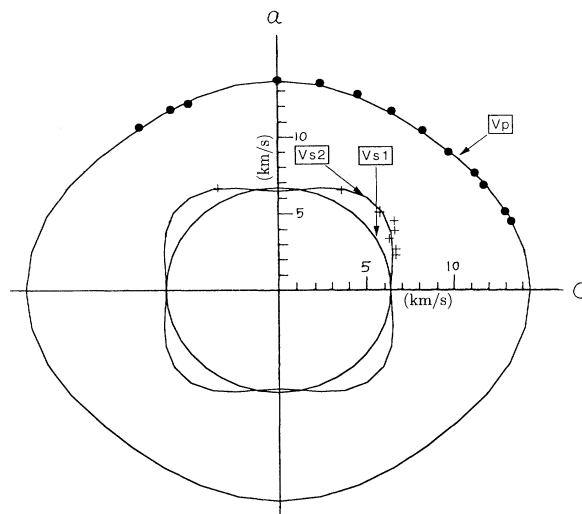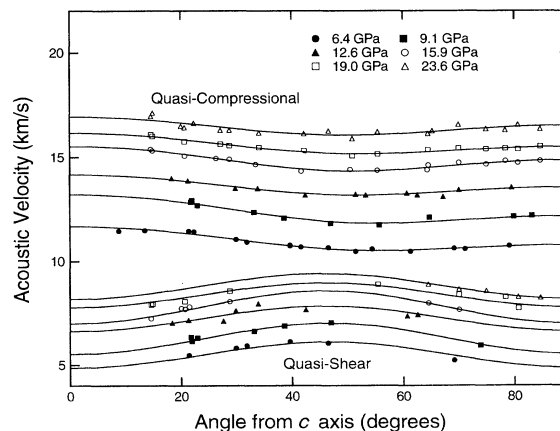

FIG. 4. Phonon velocities in single-crystal hydrogen as a function of pressure. The symbols show measured quasi-compressional and quasi-shear velocities as a function of angle from the unique crystallographic axis. The solid curves are obtained from the best-fit elastic constants at each pressure. Above 15 GPa, results from both crystals are included.

are constant for a hexagonal crystal) by changing the ω and χ angles, the refractive index of n-H_2 in this plane was constrained (Fig. 5). At $P > 10$ GPa, the present results lie systematically below those of Ref. 27 who combined data from a single spectrum, thereby neglecting possible effects of both acoustic and optical anisotropy. Although the present results overlap the previous Brillouin data within their mutual uncertainties, the new data are considered to be more reliable because we have accounted for the acoustic anisotropy. The Brillouin data below 5.4 GPa are for fluid H_2. Also shown in the figure are fits to index data obtained from the measurement of interference fringes at 5 K.[39,40] The fit reported in Ref. 40 also included the index of refraction measurements reported by Shimizu et al., which have considerably smaller uncertainties than do the interference fringe data.

IV. SINGLE-CRYSTAL ELASTIC MODULI

The relationship between the acoustic velocity, crystallographic direction, and the elastic constants of a hexagonal crystal are given by the following:[41]

$$\rho V_P^2 = \frac{A+B}{2} , \tag{2}$$

$$\rho V_{S1}^2 = \tfrac{1}{2}(C_{11}-C_{12})\sin^2\varphi + C_{44}\cos^2\varphi , \tag{3}$$

$$\rho V_{S2}^2 = \frac{A-B}{2} , \tag{4}$$

where A and B are given by

$$A = C_{11}\sin^2\varphi + C_{33}\cos^2\varphi + C_{44} , \tag{5}$$

$$B^2 = [(C_{11}-C_{44})\sin^2\varphi + (C_{44}-C_{33})\cos^2\varphi]^2$$
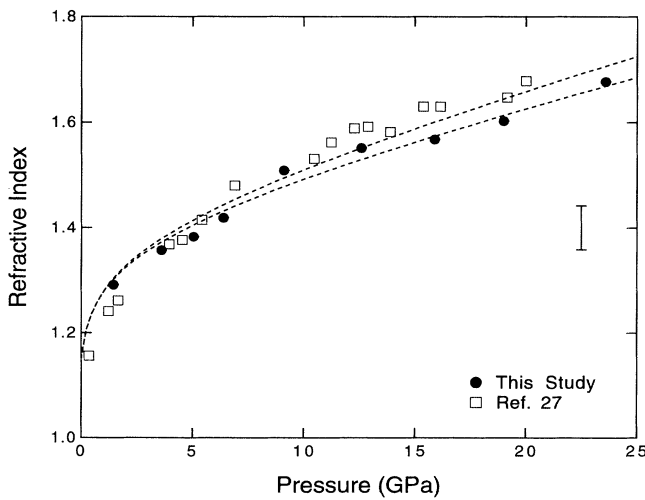$$+ (C_{13}+C_{44})^2\sin^2 2\varphi . \tag{6}$$

FIG. 5. Refractive index of n-H_2. The solid symbols are measurements for phonons in the a plane. The open symbols are from Ref. 27. The lines are fits to the data reported in Refs. 39 and 40. The uncertainty (2σ) in the refractive index determinations is shown by the error bar to the right.

In the above expressions, φ is the angle between the phonon direction and the c crystal axis, ρ is the density, V_P, V_{S1}, and V_{S2} are the quasi-compressional, pure shear, and quasi-shear velocities, respectively, and the C_{ij}'s are the five independent elastic constants which characterize crystals of hexagonal symmetry.

Since no pure shear modes were obtained, the Brillouin data yield no direct information on the modulus C_{12}. For hexagonal crystals, expressions for the linear compressibilities can be used to derive the following equation relating C_{12} to the other elastic constants through the pressure dependence of the c/a ratio:[42]

$$C_{12} = \frac{[\partial \ln(c/a)/\partial P](2C_{13}^2 - C_{11}C_{33}) - C_{11} + C_{13} + C_{33}}{1 + [\partial \ln(c/a)/\partial P]C_{33}} . \tag{7}$$

In the case of hydrogen, the pressure dependence of c/a is $1.63 - 0.000\,441P$ (GPa) between 5 and 42 GPa.[5,7] Use of this relation reduces the number of independent elastic moduli by one and enables the full set of elastic constants to be obtained from the present data. Note that if c/a is independent of pressure

$$C_{33} + C_{13} = C_{11} + C_{12} . \tag{8}$$

For hydrogen, including the contribution due to the c/a ratio increases the value of C_{12} by 2% (at 6.4 GPa) to 9% (at 23.6 GPa) and the effect on the bulk modulus is 0.5 and 1.3% at the same pressures. Thus, even when the c/a ratio is only a weak function of pressure, significant errors can be introduced into C_{12} by neglecting to take this factor into account, especially at high pressure. Other studies of hydrogen elasticity at low P and T have used Eq. (8) for determining the value of C_{12}.[38,43,44]

Initially, the densities required for Eqs. (2)–(4) were obtained from the x-ray-diffraction equation of state,[45] and these were then adjusted to obtain a self-consistent result by using the iterative data reduction scheme described below. The procedure for solving Eqs. (2)–(7) for the elastic constants first involved extensive parameter searches through elastic constant space. The C_{ij}'s were varied systematically and the goodness-of-fit determined from

$$\chi^2 = \sum_{i=1}^{N} \left[\frac{\rho V_i^{2(\text{meas})} - \rho V_i^{2(\text{calc})}}{\sigma_i} \right]^2 , \tag{9}$$

where N is the total number of measurements at a given pressure and σ is the experimental uncertainty associated with each measurement. The parameter searches were conducted with successively finer grid spacings down to 0.1 GPa. The final set of elastic constants were obtained using nonlinear least-squares inversion[46] using the results of the parameter searches as starting models. The elastic constants obtained from the inversions did not differ significantly from those found by parameter searches. The experimental uncertainties were assumed to be 1% for P waves and 2% for S waves at all pressures.

The final set of elastic constants for H_2 is shown in Fig. 6 and the numerical values listed in Table I. While the number and distribution of quasi-shear modes is limited,
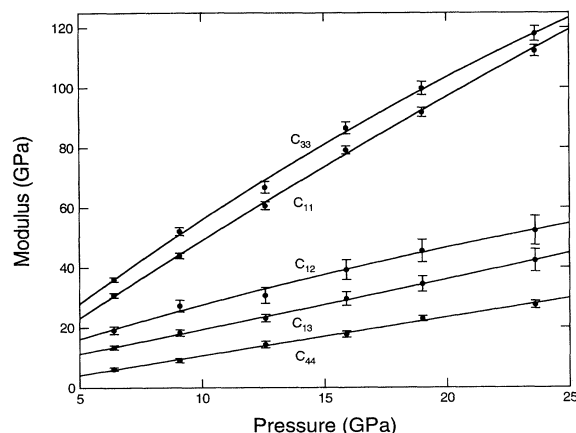
FIG. 6. Elastic constants of hydrogen as a function of pressure. The solid curves are quadratic fits to the data. Uncertainties are two standard deviations.

only a few quasi-shear modes are needed to fully constrain the constants C_{11}, C_{13}, C_{33}, and C_{44} when the quasi-compressional velocities are well distributed.[47] Velocities calculated using the best-fit elastic constants are shown in Figs. 3 and 4. The rms deviation between the calculated and measured velocities ranges from 0.074 km/s (at 15.9 GPa) to 0.141 km/s (at 23.6 GPa). The anisotropy of the quasi-compressional waves decreases from 11% at 6.4 GPa to 6% at 23.6 GPa. The quasi-shear acoustic anisotropy decreases from 23 to 14 % over the same pressure range. Here the acoustic anisotropy is defined as the difference between the maximum and minimum velocity at a given pressure divided by the average velocity at that pressure.

The elastic constants of H_2 have been reported from neutron scattering,[43] Brillouin scattering,[38] and ultrasonic[44] experiments at low P (0.1–20 MPa) and T (4.2–13.2 K), and have been calculated at ambient pressure and $T=0$ K using the self-consistent phonon approximation.[48] The low-pressure, low-temperature anisotropy of H_2 is 14–19 % for quasi-compressional waves and 20–33 % for quasi-shear waves from these studies. Thus, the acoustic anisotropy of H_2 is significantly reduced by the application of pressure. Another distinction between the present results and the low P,T data is the relative magnitudes of the moduli C_{13} and C_{44}. We find that C_{13} is larger than C_{44} by a factor of 2.2 at 6.4 GPa decreasing

to a factor of 1.5 at 23.6 GPa. At low-temperature and -pressure conditions, however, C_{44} is larger than C_{13} by a factor of 2, whereas the relative magnitudes of the other elastic constants are in agreement at low and high pressures.

Aggregate values for the bulk (K_S) and shear (G) modulus and Poisson's ratio (σ) were obtained from the individual elastic constants using the Voigt-Reuss-Hill averaging method[49] [Fig. 7(a) and Table II]. The bulk modulus increases by more than a factor of 3 and the shear modulus increases by more than a factor of 4 across the pressure range of this study. In Fig. 7(b), the aggregate elastic moduli, K_S, G, and $C_L=K_S+4G/3$, are plotted as functions of molar volume. Also shown are elastic
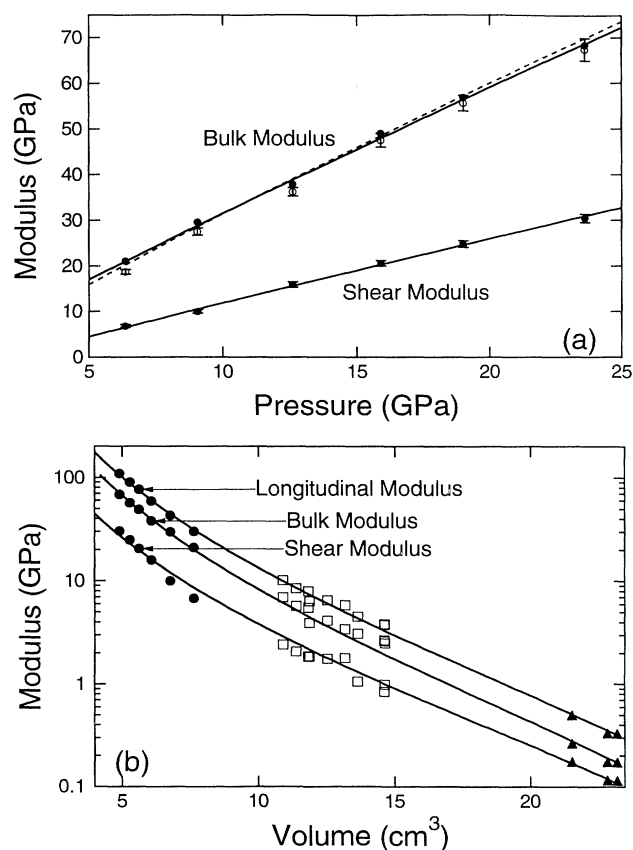

FIG. 7. (a) Aggregate bulk and shear modulus of H_2 as a function of pressure. Solid lines are quadratic fits to the data and the dashed line shows the isothermal bulk modulus of H_2 determined from the x-ray-diffraction equation of state (Ref. 45). The open symbols show the isothermal bulk modulus, K_T, obtained from the adiabatic modulus using Debye theory. Error bars for the adiabatic bulk modulus have been deleted for clarity and are nearly the same magnitude as those for K_T. (b) Aggregate elastic moduli of solid H_2 as a function of molar volume. Solid curves are fits to the data using Vinet-type equations. Solid circles, this study; boxes, Ref. 50; triangles, Refs. 38 and 44.

TABLE I. Second-order elastic moduli of n-H_2 at high pressure (295 K). Uncertainties are one standard deviation.

P(GPa)	C_{11}(GPa)	C_{12}(GPa)	C_{13}(GPa)	C_{33}(GPa)	C_{44}(GPa)
6.4	30.7(4)	19.2(6)	13.5(3)	36.0(4)	6.2(3)
9.1	44.0(5)	27.2(10)	18.3(5)	52.1(7)	9.1(3)
12.6	60.6(7)	30.7(13)	23.1(6)	66.8(10)	14.4(6)
15.9	79.3(7)	39.2(17)	29.6(12)	86.6(10)	17.7(5)
19.0	91.8(8)	45.5(19)	34.5(13)	99.8(11)	23.0(4)
23.6	112.2(10)	52.3(24)	42.3(19)	117.9(13)	27.5(6)

TABLE II. Aggregate elastic properties of n-H$_2$ at high pressure (295 K).

P (GPa)	ρ (g/cm^3)	K_S (GPa)	G (GPa)	σ	V_P (km/s)	V_B (km/s)	V_S (km/s)
6.4	0.2639	21.1(2)	6.8(2)	0.354(3)	10.69(8)	8.94(7)	5.08(6)
9.1	0.2973	29.7(4)	10.0(2)	0.348(3)	12.05(9)	10.00(8)	5.81(7)
12.6	0.3316	38.0(4)	15.9(3)	0.316(3)	13.37(9)	10.70(8)	6.93(7)
15.9	0.3586	49.1(8)	20.5(3)	0.316(4)	14.61(11)	11.70(11)	7.57(7)
19.0	0.3810	56.9(9)	24.8(4)	0.310(3)	15.37(11)	12.22(11)	8.07(7)
23.6	0.4107	68.4(13)	30.4(4)	0.306(4)	16.30(13)	12.91(14)	8.61(7)

moduli from sound velocity measurements in hydrogen at low temperature and pressure.[38,44,50] The moduli from Ref. 50 were obtained from ultrasonic longitudinal sound velocity measurements and melting slope determinations, which constrain the Debye temperature and were used to infer V_S.

Analysis of x-ray-diffraction data for H$_2$ has shown that the Vinet equation[51] provides a useful functional form for fitting H$_2$ equation-of-state data over a very wide range of compression.[45] Differentiating the Vinet equation yields the following relationship for the isothermal bulk modulus, K_T:[51]

$$K_T = (K_{0T}/x^2)[2 + (\eta - 1)x - \eta^2 x^2]\exp[\eta(1-x)] , \quad (10)$$

where $x = (V_S/V_{0S})^{1/3}$, V_S is the molar volume, $\eta = 1.5[(\partial K_{0T}/\partial P)_T - 1]$, and the subscript 0 refers to ambient pressure conditions. Analogous expressions for other elastic moduli can easily be constructed by replacing K_{0T} and its pressure derivative with the appropriate modulus and pressure derivative. Nonlinear least-squares fits to the data of Fig. 7(b) (excluding the data of Ref. 50) using such relations are also shown in the figure. While the analogous expressions are without rigorous theoretical justification (except at $T=0$ K for K_S), they provide an excellent fit to the data over the entire range of compression. The fit parameters for the adiabatic bulk modulus [$K_{0S}=0.170(3)$ GPa, $\partial K_{0S}/\partial P = 7.12(4)$ for V_{0S} constrained to be 23.22 cm^3/mol] are similar to those obtained for the isothermal bulk modulus from Vinet equation fits to pressure-volume data,[45] but are very sensitive to the assumed V_{0S}.

In the above calculations, low-T data at or near ambient pressure have been combined with room T, high-P data without explicitly accounting for effects due to temperature and rotational state. All the low-P, -T elasticity data are for parahydrogen ($J=0$) with the exception of Ref. 44 which primarily studied n-H$_2$ (ortho-para mixture with 0.75 mol fraction ortho). At low P and T, ortho-para concentration was found to have only a small effect on the measured elastic constants.[44] In Sec. V, the constant-volume temperature derivative of the isothermal bulk modulus at 295 K computed using a Debye model will be shown to be small (-0.004 GPa/K). For the present analysis, the constant-volume derivatives of the moduli in Fig. 7(b) are assumed to be zero. The value of V_{0S} used in Eq. (10) was taken from the data of Ref. 38, also without correcting for composition effects. The significance of orthopara concentration on the equation of state has been discussed by Refs. 45 and 52.

Values for Poisson's ratio at 6–24 GPa and 300 K ($\sigma=0.35$–0.30) are comparable to 0.5–1.9 GPa values from Ref. 50 at 75–164 K ($\sigma=0.30$–0.36) but are much greater than values at 0.1–20 MPa and 4.2–13.2 K ($\sigma=0.23$).[38,44] It is surprising that Poisson's ratio decreases with increasing pressure over the range of the present experiments, as this quantity normally increases with both temperature and pressure, and at 6 GPa is significantly greater than its ambient pressure, low-temperature value.

The variation of the aggregate compressional (V_P), bulk (V_B), and shear (V_S) velocities with pressure and density is shown in Fig. 8. Also shown in Fig. 8(a) are the compressional and shear velocities from the previous Brillouin study which were analyzed without structural data.[27] Between 6.4 and 23.6 GPa, the density of H$_2$ increases by 55% and from ambient pressure, $\rho/\rho_0=4.7$, which is the largest range of compression over which the elasticity of any material has been studied. Nearly linear variation of the compressional, bulk, and shear velocities with density is observed [Fig. 8(b)] for the present high-pressure data, indicating that Birch's Law[53,54] remains a suitable approximation. However, when lower-pressure (and temperature) data are included, a significant departure from Birch's Law is evident for the bulk velocity and to a lesser extent for the compressional velocity. The shear velocity displays a remarkably linear variation with density over the entire density range (0.08–0.41 g/cm^3) accessed in laboratory experiments. This is surprising in view of the fact that the theoretical justification for Birch's Law is derived largely for the bulk rather than the shear velocity.[55]

V. THERMODYNAMIC PROPERTIES

The acoustic properties of solid hydrogen are important for characterizing thermodynamic states which are not directly measurable, such as those encountered in the interiors of the Jovian planets, as well as for understanding higher pressure phase transitions, including metallization. Thermodynamic properties were determined using a Debye model.[56] At each pressure, the mean velocity, V_m, was computed by averaging over the three reciprocal velocity surfaces:

$$\frac{3}{V_m^3} = \int \left[\frac{1}{V_P^3} + \frac{1}{V_{S1}^3} + \frac{1}{V_{S2}^3} \right] d\Omega , \quad (11)$$

where $d\Omega$ is an element of solid angle. The Debye temperature was then obtained using $\theta_D = h/k(3N/$

$4\pi V_S)^{1/3}V_m$, where h is Planck's constant, k is Boltzmann's constant, and N is Avogardo's number. The mode Gruneisen parameter γ was obtained using

$$\gamma = \frac{\partial \ln V_m}{\partial \ln \rho} + \frac{1}{3} . \tag{12}$$

The resulting values of θ_D and γ are displayed in Fig. 9 and Table III. Also shown in Fig. 9(a) are values of θ_D from other elasticity and calorimetric measurements on solid hydrogen. The experimental Debye temperatures are slightly larger than the results of previous thermodynamic models for solid hydrogen which were derived from the frequency of the optic mode determined by Raman spectroscopy.[45,57] Dense hydrogen appears to have the highest θ_D of any material studied to date.

The Gruneisen parameter from Brillouin scattering is compared in Fig. 9(b) to the longitudinal optic (LO) and transverse optic (TO) mode Gruneisen parameters obtained from the volume dependence of the infrared[14,58]

and Raman[13,17,18,59] phonon frequencies measured over a broad pressure and temperature range. Also shown is the $T=0$ K Gruneisen γ from low-pressure (0–2.1 GPa) specific-heat measurements[60] and the γ value derived from the volume dependence of the longitudinal phonon at 13.2 K and 0.1–20 MPa (1–200 bars).[44] Although possible temperature dependence of γ is ignored, the Gruneisen parameter from sound velocity measurements appears significantly larger than values from calorimetric measurements or optic mode frequencies. The difference between the acoustic and optic Gruneisen parameters, however, decreases with increasing pressure.

The Mie-Gruneisen model is widely used to relate equations of state under varying thermodynamic conditions, and has frequently been applied to dense solid hydrogen.[2] An important parameter in this model is the product of density and Gruneisen parameter, $\rho\gamma$, which is often assumed to be constant for metals and ionic solids. Over the pressure range of the current experiments, the product $\rho\gamma$ increases from 0.48 to 0.55 g/cm^3. The low-T longitudinal sound velocity data of Ref. 44 yield a lower value for $\rho\gamma$ of 0.26 g/cm^3. This is consistent with the trend observed here, although the effect of temperature and the effect of the transverse phonons
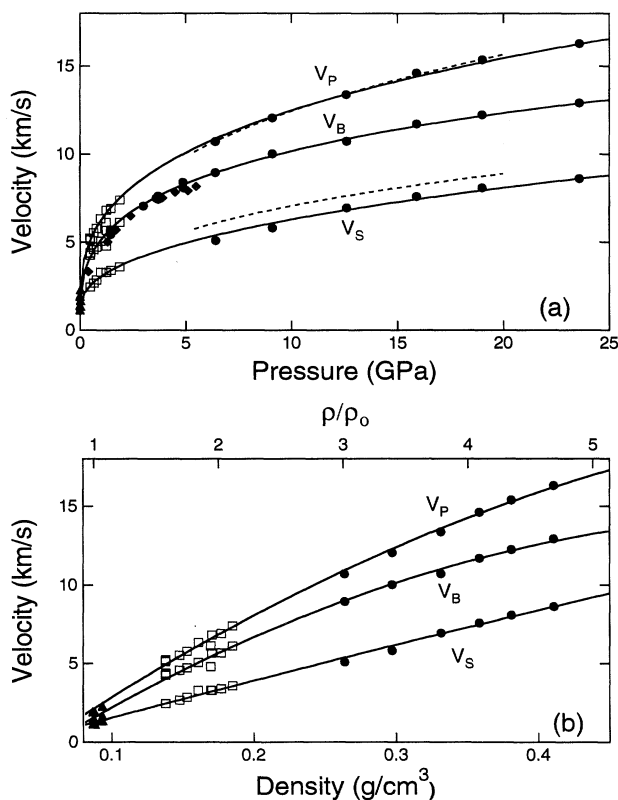

FIG. 8. (a) Aggregate V_P, V_S, and V_B for solid n-H$_2$ as a function of pressure, together with lower-pressure determinations. The dashed lines show the solid phase data of Ref. 27. Some additional data for fluid hydrogen ($P < 5.4$ GPa) obtained in this work (using a different sample than for the solid phase measurements) as well as the fluid phase data of Ref. 27 (diamonds), are also shown. The solid lines are fits of the form $V_{P,B,S} = a_0 + a_1\ln P + a_2(\ln P)^2$. (b) V_P, V_S, and V_B for solid n-H$_2$ as a function of density. Symbols are the same as for Fig. 7(b). Solid lines are quadratic least-squares fits to the data.
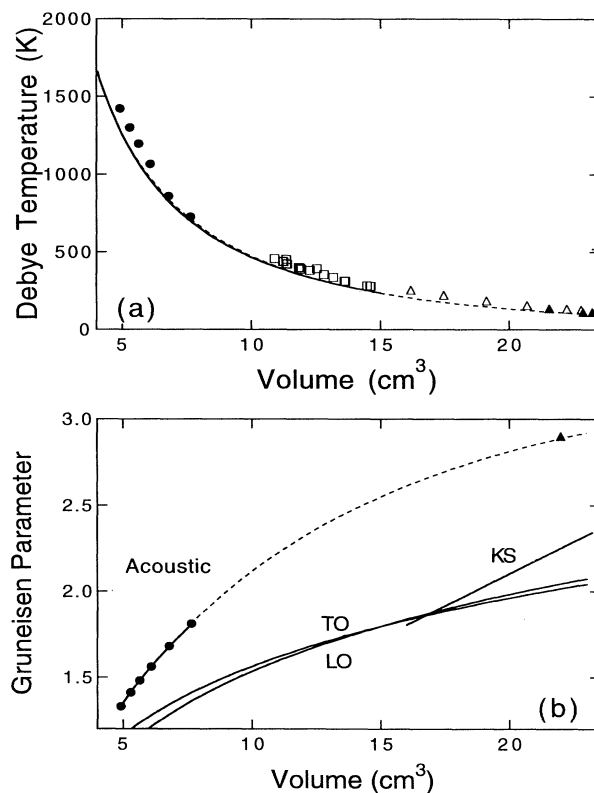

FIG. 9. Thermodynamic properties of solid n-H$_2$ as a function of molar volume. (a) Debye temperature. Open triangles, Ref. 60. The solid and dashed curves are from fits to E_{2g} optical phonon data (Refs. 45 and 57). (b) Gruneisen parameter. KS refers to Ref. 60. The other symbols are the same as Fig. 7. See text for further details.

TABLE III. Thermodynamic properties of n-H_2 at high pressure (295 K).

P (GPa)	V_m (km/s)	θ_D (K)	γ	C_V (J/mol K)	K_T (GPa)	C_P/C_V	α (10^{-6} K^{-1})
6.4	5.68	724	1.81	18.9	18.7	1.13	239
9.1	6.46	858	1.68	17.0	27.6	1.08	153
12.6	7.73	1064	1.56	14.2	36.3	1.05	100
15.9	8.45	1194	1.48	12.5	47.6	1.03	69
19.0	9.01	1300	1.41	11.2	55.7	1.02	54
23.6	9.65	1421	1.33	9.9	67.4	1.02	40

has not been included in the data of Ref. 44.

From the Debye temperature, the lattice specific heat at constant volume, C_V, was obtained by integrating the Debye function (Table III).[2] The correction from the adiabatic to the isothermal bulk modulus was then made using $K_T = K_S - \rho C_V \gamma^2 T$. The ratio of the specific heats at constant pressure and volume, C_P/C_V, was obtained from

$$C_P/C_V = 1 + \rho C_V \gamma^2 T/K_T \ . \tag{13}$$

The volumetric thermal expansion coefficient, α, was calculated from

$$\alpha = \rho \gamma C_V/K_T \ . \tag{14}$$

Both C_P/C_V and α are strongly decreasing functions of volume (Table III). Measurements of sound velocity in fluid H_2 (Ref. 61) yield values for the ratio of specific heats of 1.36 at 0.2 GPa and 1.11 at 2.0 GPa, which show that this ratio decreases strongly for the fluid phase as well. In fluid He, theoretical results[62] suggest C_P/C_V decrease from 1.510 at 0.2 GPa to 1.052 at 11.6 GPa. The present results are the first experimental derivation of this quantity at high pressure for a dense molecular solid.

Another thermodynamic parameter of interest is the product of the bulk modulus and thermal expansivity, $\alpha K_T = (\partial P/\partial T)_V$. This quantity decreases from 0.0045 GPa/K at 6.4 GPa to a value of 0.0027 GPa/K at the final pressure of 23.6 GPa. From this, the intrinsic temperature derivative of K_T can be obtained through

$$\left[\frac{\partial K_T}{\partial T} \right]_V = K_T \left[\frac{\partial(\alpha K_T)}{\partial P} \right]_T . \tag{15}$$

By fitting the αK_T data to a quadratic function of pressure, we obtain values for the intrinsic temperature derivative of n-H_2 between -0.003 and -0.005 GPa/K with no clear pressure dependence. From the intrinsic temperature derivative and the pressure derivative of the bulk modulus, $(\partial K_T/\partial P)_T$, the temperature dependence of K_T at constant pressure (and 295 K) is given by

$$\left[\frac{\partial K_T}{\partial T} \right]_P = \left[\frac{\partial K_T}{\partial T} \right]_V - \alpha K_T \left[\frac{\partial K_T}{\partial P} \right]_T . \tag{16}$$

This quantity is found to be -0.017 GPa/K at 6.4 GPa increasing to -0.012 GPa/K at the highest pressure. These values are broadly comparable to ambient pressure values for ionic and covalent solids; however, there is very little high-pressure data for comparison. For NaCl,

available compression data between 0–30 GPa and 298–773 K were used by Birch[63] to infer that $(\partial K_T/\partial T)_P$ increases from -0.015 GPa/K at ambient pressure to -0.008 GPa/K at 30 GPa, a factor of nearly 2 increase over a volume compression of about 56%. The compression achieved in H_2 between 6 and 24 GPa is 55%. The temperature dependence of the elastic moduli arises from the anharmonic nature of the lattice vibrations. A decrease in the magnitude of the temperature derivatives with pressure is the expected result of the reduction of anharmonicity with compression.

VI. EQUATION OF STATE

The isothermal P-V equation of state of H_2 was determined from

$$\ln \frac{\rho}{\rho_r} = \int_{P_r}^{P} \frac{dP'}{K_T} \ , \tag{17}$$

where P_r and ρ_r are the reference pressure and density taken from x-ray-diffraction data and K_T was fit to a quadratic function of pressure. Equation (17) was used to compute new densities which were inserted into Eqs. (2)–(7) and the process was repeated until convergence. The final densities thus obtained are independent of the assumed starting values (but not independent of the reference values).

Final values for the isothermal bulk modulus are shown in Fig. 6, and the P-ρ equation of state is shown in Fig. 10. We also compare the equation of state determined previously from x-ray-diffraction data to 26.5 GPa,[5,45] as well as more recent measurements to 42 GPa.[7] The Brillouin data yield an equation of state that is slightly more compressible than that found using the x-ray data alone, although the equations of state overlap within their mutual uncertainties. By combining our refractive index and optical thickness determinations, we find that the sample thickness at 6.4 GPa was ~ 31 μm and was reduced to ~ 19 μm at 23.6 GPa. No change in the lateral sample dimensions (about 120 μm $\times$ 80 μm) was detectable. The resulting volume change is approximately consistent with that calculated from the equation of state. The Brillouin and x-ray equations of state are significantly softer than that predicted using a pair potential derived from shock-wave data.[64]

The equation of state of H_2 obtained from the present study differs from that obtained using previous Brillouin data[27] which was more compressible, as shown in Fig. 10. The acoustic velocities measured by Ref. 27, which were
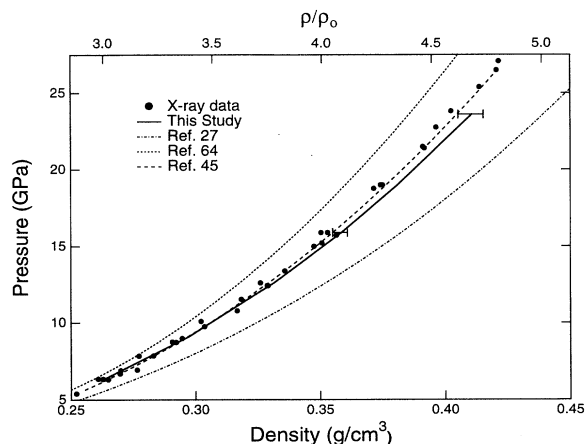
FIG. 10. Comparison of P-V equations of state of hydrogen. The solid curve is the equation of state of pure n-H_2 determined from this study using Brillouin and x-ray-diffraction data. Also shown are data points and equation of state (long-dashed line) from synchrotron x-ray data (Refs. 5, 7, and 45). The dash-dotted line shows the pressure-density relation from previous Brillouin data (Ref. 27), which did not take elastic anisotropy into account. The short-dashed line is the 300-K equation of state computed using a pair potential derived from shock-wave data (Ref. 64).

assumed to represent those of a polycrystalline aggregate, fall within the range of velocities measured in this study. The compressional velocities of Ref. 27 agree with our results, but the aggregate shear velocities are much larger [Fig. 8(a)]. By neglecting the elastic anisotropy and by not including the pure shear mode, the bulk modulus predicted in Ref. 27 was low. This illustrates the importance of determining the full set of elastic moduli in anisotropic crystals for equation-of-state determinations.

Finally, we examine the effect of possible impurities on these results. In the previous Brillouin study of fluid H_2 at high pressure,[27] the acoustic velocity was observed to decrease at a rate of 0.1 km/s/day, suggesting significant diffusion of steel gasket material into H_2 may have occurred. X-ray diffraction of H_2 samples in the diamond cell also reveal dissolution of fluid hydrogen into the gasket material (e.g., Refs. 65 and 66). However, in the present experiments, the H_2 sample was solidified immediately after loading and was held in the fluid state in the sample chamber for a total of less than 10 min. The sample chamber was also purged three times with a flush pressure of 0.0345 GPa to remove residual air from the system. Nevertheless, we consider whether the small difference between the Brillouin and x-ray equations of state could be attributable to incorporation of a small

amount of impurity (e.g., rhenium gasket material, H_2O, N_2) into the H_2 sample. To investigate this possibility, we performed an inversion of Eqs. (2)–(7) and (17) in which the molar volume of the sample was fixed at the x-ray-diffraction value but the molecular weight was allowed to vary. In this way, the reference density used in Eq. (17) could change after each iteration. In this case, the inversion converged to a single molecular weight of 2.11 (0.01) g/mol, which is 4.7% larger than the value for pure H_2. This could be explained, for example, by the incorporation of 0.03-mol % Re impurity. While we believe that contamination by the gasket material is not a likely explanation for the small difference between the x-ray and Brillouin equations of state, this illustrates use of the Brillouin technique for studying possible pressure-induced chemistry in hydrogen mixtures and characterization of possible impurity contents in the solid at very high pressures.

VII. CONCLUSIONS

A technique that combines Brillouin scattering and synchrotron x-ray diffraction of low-Z materials has enabled us to measure the high-pressure elastic constants of a hexagonal single crystal over a wide range of compression. From 6 to 24 GPa, the velocity anisotropy of hydrogen was found to decrease from 11 to 6 % for quasi-compressional waves and from 24 to 14 % for quasi-shear waves. In combination with low P and T data, the elasticity of H_2 has now been investigated over a factor of 4.7 in density, the largest range investigated in any solid to date. Thermodynamic properties of H_2 were computed using a Debye model. The 295-K pressure dependencies of the Debye temperature, thermal expansivity, ratio of specific heats, and the temperature derivative of the isothermal bulk modulus were determined for the first time for solid n-H_2 using this model. The bulk modulus and equation of state determined from this data agree with previous results solely from x-ray diffraction. The effect of a small amount of contamination of the H_2 sample is examined. In the present study, data collection was discontinued after 23.6 GPa because the shear modes became very weak. However, there is no reason, in principle, why the present single-crystal technique could not be extended to significantly higher pressures.

[1]J. van Kranendonk, *Solid Hydrogen* (Plenum, New York, 1983).
[2]I. F. Silvera, Rev. Mod. Phys. **52**, 393 (1980).
[3]H. K. Mao and R. J. Hemley, Am. Sci. **80**, 234 (1992).
[4]R. J. Hemley, H. K. Mao, M. Hanfland, J. H. Eggert, C. S.

Zha, and J. F. Shu, in *Physics of Strongly Coupled Plasmas*, edited by H. M. Van Horn and S. Ichimaru (University of Rochester Press, Rochester, NY, in press).
[5]H. K. Mao, A. P. Jephcoat, R. J. Hemley, L. W. Finger, C. S. Zha, R. M. Hazen, and D. E. Cox, Science **239**, 1131 (1988).

[6]V. P. Glazkov, S. P. Besedin, I. N. Goncharenko, A. V. Irodova, I. N. Makarenko, V. A. Somenkov, S. M. Stishov, and S. S. Shilsteyn, Pis'ma Zh. Eksp. Teor. Fiz. **47**, 569 (1988) [JETP Lett. **47**, 661 (1988)].

[7]J. Hu, H. K. Mao, J. F. Shu, and R. J. Hemley (unpublished).

[8]R. J. Hemley and H. K. Mao, Phys. Rev. Lett. **61**, 857 (1988).

[9]R. J. Hemley and H. K. Mao, Phys. Rev. Lett. **63**, 1393 (1989).

[10]H. E. Lorenzana, I. F. Silvera, and K. A. Goettel, Phys. Rev. Lett. **63**, 2080 (1989).

[11]R. J. Hemley and H. K. Mao, Science **249**, 391 (1990).

[12]H. E. Lorenzana, I. F. Silvera, and K. A. Goettel, Phys. Rev. Lett. **65**, 1901 (1990).

[13]R. J. Hemley, H. K. Mao, and J. F. Shu, Phys. Rev. Lett. **65**, 2670 (1990).

[14]M. Hanfland, R. J. Hemley, H. K. Mao, and G. P. Williams, Phys. Rev. Lett. **69**, 1129 (1992).

[15]M. Hanfland, R. J. Hemley, and H. K. Mao, Phys. Rev. Lett. **70**, 3760 (1993).

[16]I. F. Silvera and R. J. Wijngaarden, Phys. Rev. Lett. **47**, 39 (1981).

[17]R. J. Wijngaarden, V. V. Goldman, and I. F. Silvera, Phys. Rev. B **27**, 5084 (1983).

[18]R. J. Hemley, J. H. Eggert, and H. K. Mao, Phys. Rev. B **48**, 5779 (1993).

[19]J. H. Eggert, K. A. Goettel, and I. F. Silvera, Europhys. Lett. **11**, 775 (1990).

[20]R. J. Hemley, M. Hanfland, and H. K. Mao, Nature **350**, 488 (1991).

[21]A. Garcia, M. L. Cohen, J. H. Eggert, F. Moshary, W. J. Evans, K. A. Goettel, and I. F. Silvera, Phys. Rev. B **45**, 9709 (1992).

[22]H. K. Mao and R. J. Hemley, Science **244**, 1462 (1989).

[23]H. K. Mao, R. J. Hemley, and M. Hanfland, Phys. Rev. Lett. **65**, 484 (1990).

[24]J. H. Eggert, F. Moshary, W. J. Evans, H. E. Lorenzana, K. A. Goettel, I. F. Silvera, and W. C. Moss, Phys. Rev. Lett. **66**, 193 (1991).

[25]M. Hanfland, R. J. Hemley, and H. K. Mao, Phys. Rev. B **43**, 8767 (1991).

[26]E. M. Brody, H. Shimizu, H. K. Mao, P. M. Bell, and W. A. Bassett, J. Appl. Phys. **52**, 3583 (1981).

[27]H. Shimizu, E. M. Brody, H. K. Mao, and P. M. Bell, Phys. Rev. Lett. **47**, 128 (1981).

[28]A. Polian, in *Frontiers of High Pressure Research*, edited by H. D. Hochheimer and R. D. Etters (Plenum, New York, 1991), p. 181.

[29]H. Shimizu and S. Sasaki, Science **257**, 514 (1992).

[30]S. A. Lee, D. A. Pinnick, S. Lindsay, and R. C. Hanson, Phys. Rev. B **34**, 2799 (1986).

[31]T. Ishidate, S. Sasaki, and K. Inoue, High Press. Res. **1**, 53 (1988).

[32]H. K. Mao and P. M. Bell, Carnegie Inst. Washington Yearb. **79**, 409 (1980).

[33]R. M. Hazen, H. K. Mao, L. W. Finger, and R. J. Hemley, Phys. Rev. B **36**, 3944 (1987).

[34]V. Diatschenko, C. W. Chu, D. H. Liebenberg, D. A. Young, M. Ross, and R. L. Mills, Phys. Rev. B **32**, 381 (1985).

[35]H. K. Mao, J. Xu, and P. M. Bell, J. Geophys. Res. **91**, 4673 (1986).

[36]R. Mock, B. Hillebrands, and J. R. Sandercock, J. Phys. E **20**, 656 (1987).

[37]C. H. Whitfield, E. M. Brody, and W. A. Bassett, Rev. Sci. Instrum. **47**, 942 (1976).

[38]P. J. Thomas, S. C. Rand, and B. P. Stoicheff, Can. J. Phys. **56**, 1494 (1978).

[39]J. van Straaten, I. F. Silvera, and R. J. Wijngaarden, Phys. Rev. Lett. **48**, 97 (1982).

[40]J. van Straaten and I. F. Silvera, Phys. Rev. B **37**, 1989 (1988).

[41]M. J. P. Musgrave, *Crystal Acoustics* (Holden-Day, San Francisco, 1970).

[42]J. P. Franck and R. Wanner, Phys. Rev. Lett. **25**, 345 (1970).

[43]M. Nielsen, Phys. Rev. B **7**, 1626 (1973).

[44]R. Wanner and H. Meyer, J. Low Temp. Phys. **11**, 715 (1973).

[45]R. J. Hemley, H. K. Mao, L. W. Finger, A. P. Jephcoat, R. M. Hazen, and C. S. Zha, Phys. Rev. B **42**, 6458 (1990).

[46]W. H. Press, B. P. Flannery, S. A. Teukolsky, and W. T. Vettering, *Numerical Recipes in C* (Cambridge University Press, New York, 1987).

[47]B. Castegnede, A. G. Every, and W. Sache, C. R. Acad. Sci. Paris **314**, 865 (1992).

[48]V. V. Goldman, J. Low Temp. Phys. **26**, 715 (1977).

[49]J. P. Watt and L. Peselnick, J. Appl. Phys. **51**, 1525 (1980).

[50]D. H. Liebenberg, R. L. Mills, and J. C. Bronson, Phys. Rev. B **18**, 4526 (1978).

[51]P. Vinet, J. H. Rose, J. Ferrante, and J. R. Smith, J. Phys.: Condens. Matter **1**, 1941 (1989).

[52]A. Driessen and I. F. Silvera, Phys. Rev. B **35**, 6649 (1987).

[53]F. Birch, J. Geophys. Res. **65**, 1083 (1960).

[54]A. J. Campbell and D. L. Heinz, Science **257**, 66 (1992).

[55]T. J. Shankland, Phys. Earth Planet. Int. **8**, 121 (1974).

[56]M. Born and K. Huang, *Dynamical Theory of Crystal Lattices* (Clarendon, Oxford, 1954).

[57]H. Hemmes, A. Driessen, and R. Griessen, J. Phys. C **19**, 3571 (1986).

[58]H. K. Mao, J. Xu, and P. M. Bell, in *High Pressure in Science and Technology*, edited by C. Homan, R. K. MacCrone, and E. Whalley (North-Holland, New York, 1984), p. 327.

[59]P. J. Berkhout and I. F. Silvera, J. Low Temp. Phys. **36**, 231 (1979).

[60]J. K. Krause and C. A. Swenson, Phys. Rev. B **21**, 2533 (1980).

[61]R. L. Mills, D. H. Liebenberg, J. C. Bronson, and L. C. Schmidt, J. Chem. Phys. **66**, 3076 (1977).

[62]R. Le Toullec, P. Loubeyre, and J.-P. Pinceaux, Phys. Rev. B **40**, 2368 (1989).

[63]F. Birch, J. Geophys. Res. **91**, 4949 (1978).

[64]M. Ross, F. H. Ree, and D. A. Young, J. Chem. Phys. **79**, 1487 (1983).

[65]J. V. Badding, R. J. Hemley, and H. K. Mao, Science **253**, 421 (1991).

[66]H. K. Mao, J. F. Shu, and R. J. Hemley (unpublished).